J Mater Sci: Mater Med (2011) 22:461–467
DOI 10.1007/s10856-011-4234-6

Characterization of self-organized TiO_2 nanotubes on Ti–4Zr–22Nb–2Sn alloys and the application in drug delivery system

Y. Q. Liang · Z. D. Cui · S. L. Zhu · X. J. Yang

Received: 17 September 2010 / Accepted: 11 January 2011 / Published online: 2 February 2011

Abstract In this study, the self-organized TiO_2 nanotubes grown by anodization of Ti–4Zr–22Nb–2Sn at different potentials, concentration of NH_4F and anodization time was investigated. The morphology of nanotubes was observed by FE-SEM. The drug-loaded nanotubes were also fabricated in aqueous media containing minocycline hydrochloride. They were characterized by SEM, XPS and FT-IR. The results showed that the drug of minocycline hydrochloride (MH) was loaded in the nanotubes. The release effects were studied in phosphate buffer solution (PBS). The release rate of MH from TiO_2 nanotubes with shorter tube length in PBS was lower than the one of MH from longer nanotubes. The sustaining release time could last at least 150 h. Hence, it is a promising method to eliminate the harmful reactions by carrying drug in the tubes when the titanium alloys were used as biomedical implants.

1 Introduction

Titanium and its alloys have been widely used as base materials for orthopaedic or dental implants due to its excellent biocompatibility, good load-bearing properties and good corrosion resistance [1–4]. However, problems in terms of adhesion and stability for long periods in the living body still exist [5, 6]. Therefore, various efforts are undertaken to further improve the biocompatibility and optimize the modifications of titanium surfaces. It is known that small changes in the surface properties can lead to completely different behavior of the material. Therefore, new better modifications of titanium surfaces have been established. For example, anodization at lower voltages leads to highly ordered self-organized TiO_2 nanotubular layer. In the past decades, nanoscale structures of TiO_2 have attracted increasing scientific and technological attention due to the applications in solar cells [7], water-splitting [8], and photocatalysis [9]. What's more, another important application of TiO_2 nanotube is to improve the bioactivity of titanium in biochemical filed [10–14]. The Ti base materials show a better bone-binding ability on the TiO_2 covered surface of the implants [15, 16]. It has been previously reported that TiO_2 nanotubes can improve osteoblast attachment, function and proliferation. Besides, this nanotopographical features can also be used to promote proliferation and function in endothelial cells and help vascular smooth muscle cell maintain their differentiated and non-proliferative phenotype [17, 18]. Other studies have also suggested that nanotubes can be used in vascular applications, enhancing endothelial cell production and motility [19].

In despite of this, many clinical investigations showed that titanium and its alloys used in corrosive environment like body fluid always release detrimental ions in blood stream of the patients [20, 21], which can cause severe diseases such as inflammatory, allergic or carcinogenic reactions. But drugs such as anti-inflammatory drugs, antibiotics and growth factors are not effective when delivered by systemic routes because the drug cannot readily reach the implant–tissue interface. Hence, it's crucial to keep the advantage of better bone-binding ability for the bulk titanium covered by TiO_2 nanotubes and

Y. Q. Liang · Z. D. Cui · S. L. Zhu · X. J. Yang (✉)
School of Materials Science and Engineering,
Tianjin University, Tianjin 300072, China
e-mail: xjyang@tju.edu.cn

S. L. Zhu · X. J. Yang
Tianjin Key Laboratory of Composite and Functional Materials,
Tianjin 300072, China

eliminate the harmful reactions by local drug therapy. The method that carrying drugs in the tubes can not only offer a high localized drug concentration without any systemic toxicity but also deliver drugs right at the site of implantation. Previous studies showed the antibiotic release from the nanotubes to prevent bacterial adhesion by loading gentamicin in tubes [22]. Moreover, paclitaxel is also loaded in nanotubes, which was used as an anti proliferative agent to treat inflammation, cancer, and stent restenosis [23].

However, the TiO_2 nanotubes with single-diameter structure used in local drug therapy were prepared on the substrate of pure titanium. To-date, new Ti-based alloys with non-toxic elements such as Nb, Zr, and Sn have been developed to substitute pure Ti due to their excellent properties such as high strength and reasonable elastic modulus among the metal-based biomaterials. Accordingly, in the present study, a technique of producing TiO_2 nanotubes with two-size-scale on the substrate of Ti–4Zr–22Nb–2Sn alloys by anodization, which can maintain their mechanical properties was proposed. The tube diameter and length can be easily controlled by varying the anodization potentials and time. Meanwhile, Minocycline hydrochloride (MH), a member of the tetracycline antibiotics, is useful in the treatment of a host of topical bacterial infections [24]. Hence, it was selected as the model drug in this current study, and the drug release effects of drug-loaded nanotubes were performed in phosphate buffer solution (PBS) effectively.

2 Materials and methods

TiO_2 nanotube arrays were grown from a Ti–4Zr–22Nb–2Sn substrate (0.25-mm thick, Aldrich) by anodization in an electrolyte of 0.31 M NH_4F with water/glycerol (50:50 vol.%) [25]. A two-electrode electrochemical setup consisting of the Ti substrate anode and a Pt cathode was used. Nanotube formation was achieved at potentials ranging from 10 to 56 V at room temperature. Prescribed amounts of Minocycline hydrochloride (MH) were dissolved in distilled water. The as-prepared TiO_2 nanotubes with different tube lengths were immerged in this solution and dried at room temperature. Subsequently, the nanotube mouth was closed by covering poly-lacto-co-glycolic acid (PLGA) on the tube surface. Then the nanotube loaded with drugs (MH) was formed. The release experiment in vitro was carried out according to a method reported previously [23]. The Ti–4Zr–22Nb–2Sn samples loaded with MH were enclosed by filter membrane. Each sample was immersed into 5 ml of phosphate buffer solution (PBS, 0.01 M, pH 7.4) at 37.5°C. At specific time intervals, 3 ml of medium was taken out and replaced with PBS. Three replicated samples were recorded at each time point. The sample surfaces were analyzed with a field emission scanning electron microscope (FE-SEM, Hitachi FE-SEM S-4800) equipped with an energy-dispersive X-ray analysis unit (EDS). X-ray photoelectron spectroscopy (PHL1600ESCA XPS) was also used to characterize the chemical composition of the surfaces. Fourier transform infrared (FT-IR) spectroscopy measurement was used to further confirm the formation of the MH-nanotube loaded system. The amount of MH released from the nanotubes was determined with the ultraviolet Visible Spectrophotometer (UV-2450, Shimadzu, Japan) at 360 nm.

3 Results and discussion

Generation of self-organized TiO_2 nanotubes with two-size-scale diameters was achieved by anodizing Ti–4Zr–22Nb–2Sn sheets in a 0.31 M NH_4F electrolyte with water/glycerol (50:50 vol.%) at different voltages ranging from 10 to 56 V for 3 h, thus precisely controlling tube length and bottom diameter. Figure 1 shows that the length and diameters linearly depend on the applied potential. It also clearly demonstrates that highly ordered tubular layers can be formed in a very wide potential range. This is in line with earlier experimental findings in pure titanium [26], Ti–Zr alloys [27], Ti–Zr–Nb alloys [28] and Ti–Nb–Ta–Zr [29]. As shown in the insets of Fig. 1, the resulting tube length and larger diameter formed at 56 V for 3 h can reach up to 8,807 ± 10 and 254 ± 10 nm, respectively. A linear relationship can be ascribed to the voltage influence in terms of a field-aided oxide growth model [30]. As for the nanotube length, it becomes longer at more positive potential following the larger anodic current during the nanotube formation [31]. Figure 2 shows an evaluation of the tube length in dependence of the concentration of NH_4F at 35 V for 3 h. It is obvious that the tube length first

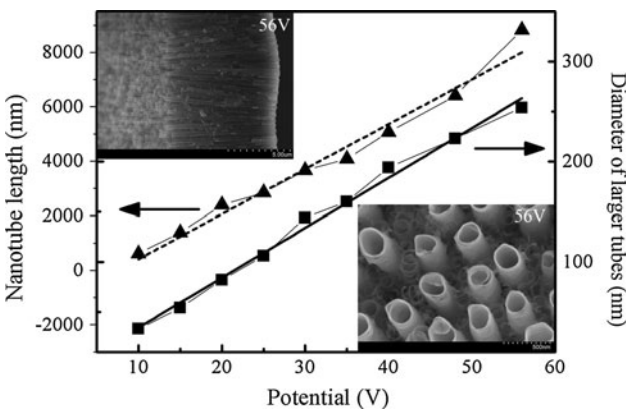

Fig. 1 Dependence of nanotube length on the anodization potential (the substrate is anodized for 3 h in this case)

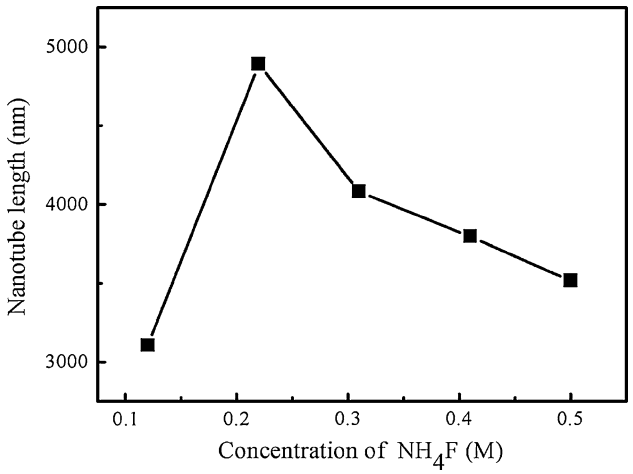

Fig. 2 Dependence of nanotube length on concentration of NH_4F when the potential is maintained at 35 V for 3 h

increases to the peak value (length of 4,889 ± 10 nm corresponding to 0.22 M NH_4F) and then decreases with increasing the NH_4F concentration. The pore formation occurs due to the localized chemical dissolution of the oxide as well as the pore mouth dissolution by F^- [32]. Therefore, the tube length is determined by the comparison between the dissolution of the tube top and the formation of the tube bottom [27]. The decrease of the length can be attributed to the accelerated chemical dissolution of the tube mouth by excessive fluoride ions in the electrolyte.

Further experiments were performed to elucidate the influence of time (0.5, 1, 2 and 3 h) on the morphology and dimension of the growing layers. Figure 3 shows the bottom and cross-sectional view from a set of anodization experiments at 35 V during 3 h using 0.31 M NH_4F electrolyte with water/glycerol (50:50 vol.%). It can be seen that the tube length increases with time from 2,128 ± 10 nm in 0.5 h to 4,080 ± 10 nm in 3 h. Meanwhile, the bottom view of the nanotubes formed in 0.5 h shows only one-size diameter. After additionally approximately 0.5 h has passed, the diameter of some tubes increases, exhibiting two-size scale diameter. It indicates that some nanotubes with faster growth rates in the growth "race" obtain the optimal electrochemical conditions, and grow to lager diameter nanotubes, while those with slower growth rates do not change significantly. By further anodization, the distribution density of larger diameter nanotubes increases gradually, which can induced that the tubes with smaller diameter will continue growing if a sufficient acidification of the pore tip can be maintained [33] after long time anodization.

After the preparation of drug-loaded nanotubes, the top-views of nanotubes before and after drug-loading were observed by SEM. Figure 4a shows a highly ordered layer that consists of densely packed nanotubes with an open top. After immersing in MH solutions, the morphology of drug-loading nanotubes was shown in Fig. 4b. The intervals between nanotubes were filled with MH, which is identified by EDS and supported by the elements of N and Cl (not shown in this paper). The nanotubes loaded with MH were further covered by PLGA to slow down the drug release. The top image of the composite coating (nanotube/MH/PLGA) can be seen in Fig. 4c. The surface of this coating is smooth and glossy and the tube structures cannot be observed. In order to additionally confirm the deposition of MH in nanotubes, FT-IR and XPS measurements were also performed.

Figure 5 shows the FT-IR spectra of TiO_2 nanotube before and after loading MH recorded in the range of 4,000–400 cm^{-1}. Two peaks at approximately 3,425 and 1,620 cm^{-1} indicate the presence of adsorbed or hydrogen-bonded water molecule on the nanotubes [34]. In addition, the band at 541 cm^{-1} in Fig. 5a was associated with the Ti–O–Ti stretching mode of TiO_2 [35]. The spectrum of MH doped nanotubes in Fig. 5b has a broad band between 1,000 and 1,600 cm^{-1}. The bands at 1143, 1476 and 1215 cm^{-1} were attributed to the C–H stretching mode [34]. The bands at 1305, 1368, 1411, 1530 and 2931 cm^{-1} was associated with the C–N stretching, Amide III + CH_3 end-group deformation, CH_2 deformation, Amide II and C–H stretching [36, 37]. The peak at 3,010 cm^{-1} is assigned to the aromatic ring (C_6H_5) [38]. The bands below 3,010 cm^{-1} are from the saturated main chain C–H groups [39]. The IR spectra show that MH is grafted into TiO_2 nanotubes.

The incorporation of MH can be further justified by the XPS spectra of N 1s and Cl 2p, as shown in Fig. 6. The high-resolution N 1s spectrum (Fig. 6a) includes peaks at binding energies 399.2 and 401.1 eV. The peak at 399.2 eV is assigned to the $–NH_2$ while the peak at 401.1 eV is attributed to protonated amine groups [40–42]. Shown in Fig. 6b are the Cl 2p spectra of MH doped nanotubes. The peaks that are observed at 197.1 and 198.2 eV can be assigned by a certain degree of surface chlorination caused by HCl [43]. Therefore, the Cl 2p spectra demonstrate the existence of HCl from MH on the nanotube surface.

To study the drug release behavior, the nanotubes prepared at 15, 25, 35, and 45 V were selected to carry MH. As shown in Fig. 7, the MH was loaded on the nanotubes with different lengths ((a) 1.5 μm at 15 V, (b) 2.8 μm at 25 V, (c) 4.1 μm at 35 V, (d) 5.7 μm at 45 V). It could be seen that the top of nanotube interface were filled with MH. The amount of loaded MH increased with the tube length and the small size tubes disappeared gradually in Fig. 7c and d. In applying MH-nanotube to a drug delivery system, the MH release needed to be fast at the initial stage to eliminate the harmful reactions cause by detrimental ions in the implant-tissue interface. The load capacity of MH was 0.002 g,

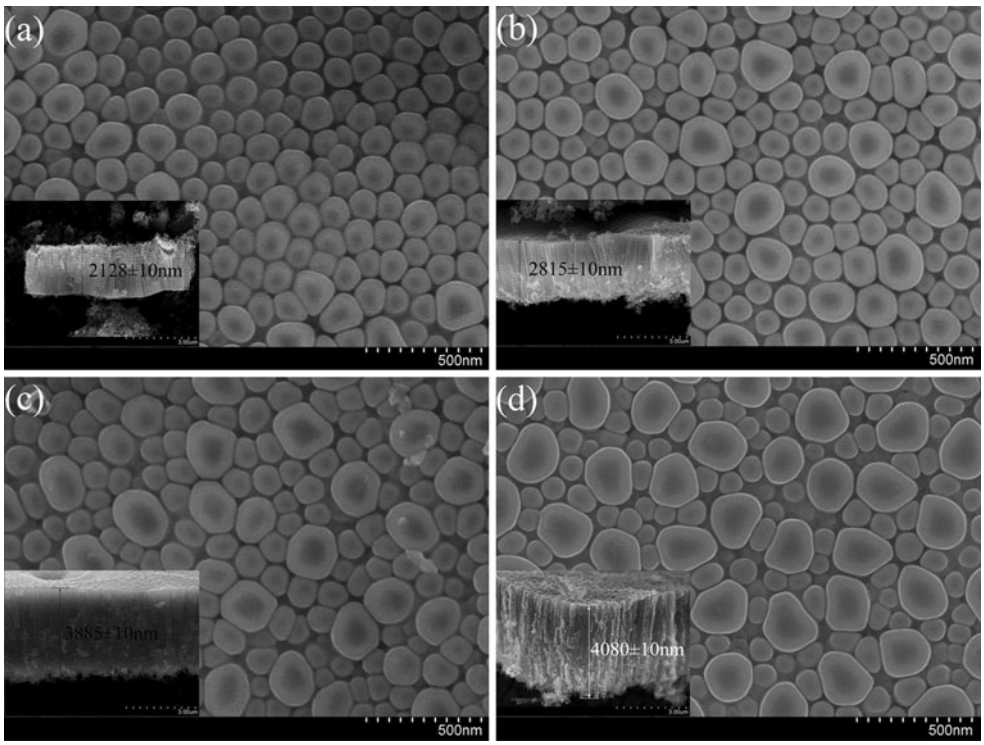

Fig. 3 SEM bottom view of nanotubes anodized for **a** 0.5 h, **b** 1 h, **c** 2 h and **d** 3 h in water/glycerol/0.31 M NH_4F at 35 V (the *insets* shows the cross-sectional images)

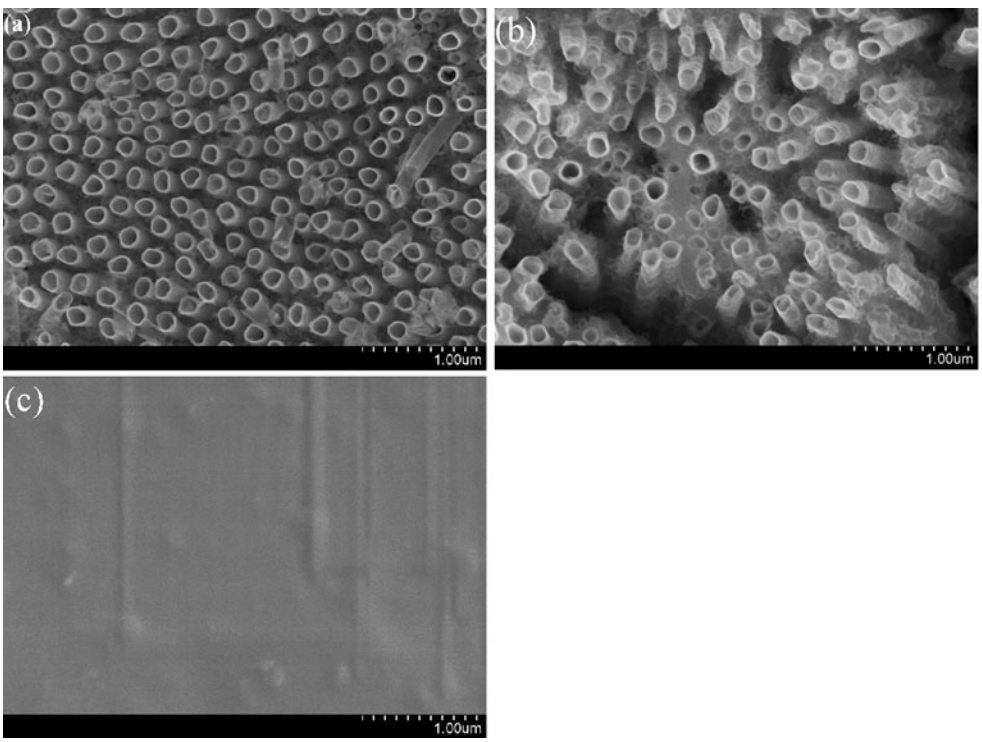

Fig. 4 SEM top view of **a** as-formed nanotubes formed in water/glycerol/0.31 M NH_4F at 35 V for 3 h, **b** MH-loaded nanotubes and **c** MH-loaded nanotubes covered by PLGA

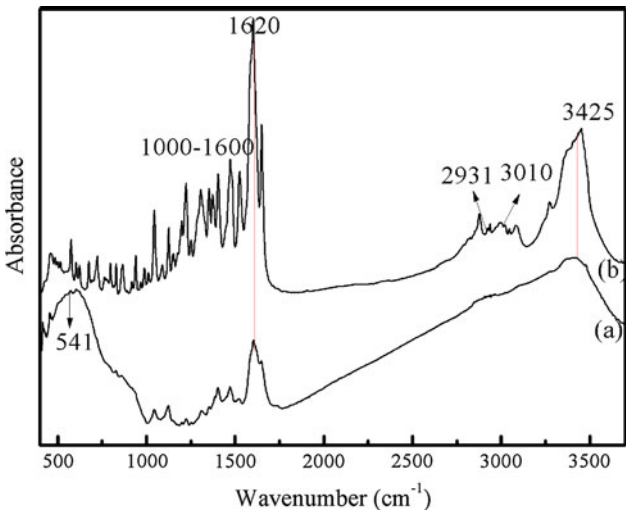

Fig. 5 FT-IR spectra of (*a*) as-formed nanotubes and (*b*) MH-loaded nanotubes

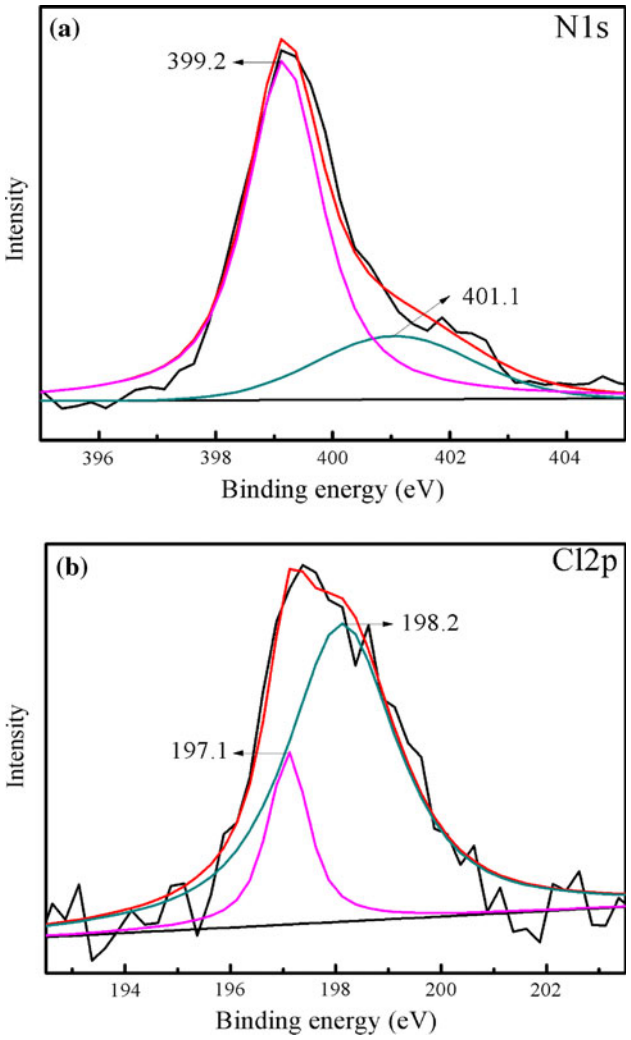

Fig. 6 High-resolution XPS spectra of **a** N 1s and **b** Cl 2p of the surface of MH-loaded nanotubes

which was obtained by the weight difference of nanotubes before and after drug loading. The release profiles of the samples of MH-nanotube into the surrounding aqueous phase were shown in Fig. 8. The inset was the UV–visible absorption spectra of the MH solution. The spectra showed that MH had a broad and continuous absorption at 360 nm. We found that the release rate of MH from TiO_2 nanotubes with shorter tube length (see Fig. 8a, b) in PBS was lower than the one of MH from longer nanotubes (see Fig. 8c, d). With the first phase lasting about 7 h, 10.3, 19.7, 19.5, and 43.4% of loaded MH was released from TiO_2 nanotubes with different tube lengths ((a) 1.5 μm, (b) 2.8 μm, (c) 4.1 μm, (d) 5.7 μm), respectively. The (d) sample was considered to be a burst effect, and it had been attributed to the excess of MH on the surface of nanotubes as shown in Fig. 7d. As demonstrated in Fig. 8, the sustaining release time of nanotubes was at least 150 h, which had longer sustaining release time than that in the colloidal delivery system [44], nanospheres [45] and carbon nanohorns [46]. The factor that affected the drug release rate significantly was the higher aspect ratio of nanotubes, which could effectively retard the drug release. The accumulative release efficiencies of MH-nanotube ((c) 4.1 μm) and MH-nanotube ((d) 5.7 μm) could reach up to 90.7 and 87.9% within 194 h, respectively. Compared with Fig. 8c and d, a and b had relatively lower release efficiencies of 48.2 and 59.1%. This was because the MH was easier to permeate into shorter nanotubes than longer ones. Therefore, the MH mainly accumulated on the top of longer nanotubes, but only small amount of MH was observed on the surface of shorter tubes. Results indicated that the longer nanotubes had a promoting function for drugs release; that is, the release rate can be controlled by varying the nanotube length. A faster and more complete release can be obtained for sample of MH-nanotube (5.7 μm) in Fig. 8d, which demonstrated that longer nanotubes loaded with MH is preferable to used as biomedical implants.

4 Conclusions

In this study, the self-organized TiO_2 nanotubes with two-size-scale diameters are fabricated by anodizing Ti–4Zr–22Nb–2Sn sheets at different voltages ranging from 10 to 56 V. The tube lengths and diameters linearly depend on the applied potential. The tube length is also affected by the concentration of NH_4F and anodization time. With the increasing time, the distribution density of larger diameter nanotubes increases correspondingly. The Minocycline hydrochloride (MH) can be loaded in the nanotubes successfully. The release rate of MH from TiO_2 nanotubes with shorter tube length in PBS is lower than the one of MH from longer nanotubes. The burst release of MH

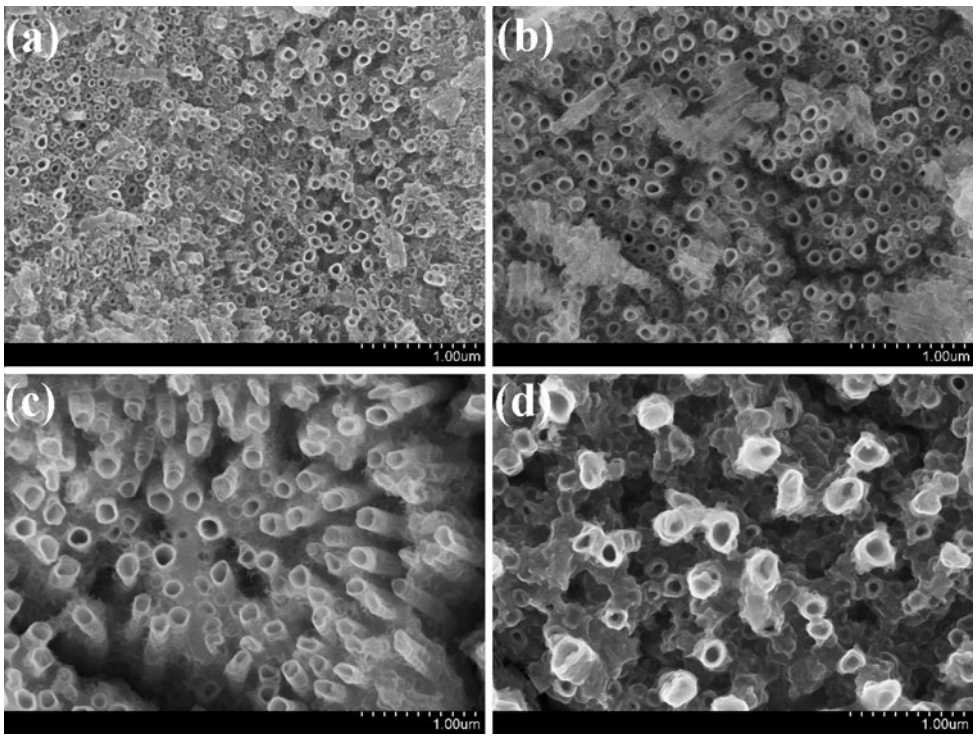

Fig. 7 SEM top view of nanotubes loaded with MH, the nanotubes were prepared at the potentials of 15, 25, 35, 45 V, corresponding to the tube lengths of **a** 1.5 μm, **b** 2.8 μm, **c** 4.1 μm, **d** 5.7 μm in Fig. 1

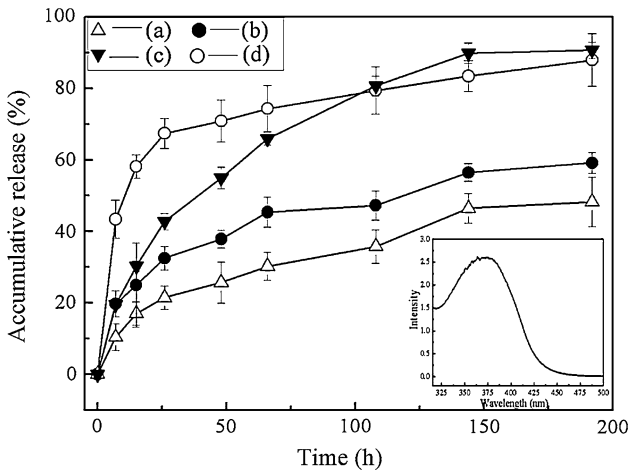

Fig. 8 MH release profiles from self-organized nanotubes in PBS (pH 7.4, 37°C), the four curves are corresponding to the samples in Fig. 7

from longer nanotubes is obvious due to the excess of MH on the surface of nanotubes, which is in line with the requirement that the release of MH needs to be fast at the initial stage. The sustaining release time of nanotubes is at least 150 h. Hence, the drug release can be effectively retarded due to the higher aspect ratio of nanotubes.

Acknowledgments This work was supported by Key Project in the Science and Technology Pillar Program of Tianjin (09ZCKFGX 29100), Natural Science Foundation of Tianjin (08JCYBJC08900) and National Natural Science Foundation of China (50901051). The infra-structural supports from the Tianjin University are also acknowledged.

References

1. Cacciafesta P, Hallam KR, Watkinson AC, Allen GC, Miles MJ, Jandt KD. Visualisation of human plasma fibrinogen adsorbed on titanium implant surfaces with different roughness. Surf Sci. 2001;491:405–20.
2. Kasemo B. Biological surface science. Surf Sci. 2002;500: 656–77.
3. Liu Q, Ding J, Mante FK, Wunder SL, Baran GR. The role of surface functional groups in calcium phosphate nucleation on titanium foil: a self-assembled monolayer technique. Biomaterials. 2002;23:3103–11.
4. Liu DP, Majewski P, O'Neill BK, Ngothai Y, Colby CB. The optimal SAM surface functional group for producing a biomimetic HA coating on Ti. J Biomed Mater Res A. 2006;77A: 763–72.
5. Jarcho M. Calcium-phosphate ceramics as hard tissue prosthetics. Clin Orthop Relat Res. 1981;157:259–78.
6. Hench LL. Bioceramics—from concept to clinic. J Am Ceram Soc. 1991;74:1487–510.
7. Mor GK, Shankar K, Paulose M, Varghese OK, Grimes CA. Use of highly-ordered TiO_2 nanotube arrays in dye-sensitized solar cells. Nano Lett. 2006;6:215–8.
8. Park JH, Kim S, Bard AJ. Novel carbon-doped TiO_2 nanotube arrays with high aspect ratios for efficient solar water splitting. Nano Lett. 2006;6:24–8.
9. Ghicov A, Schmidt B, Kunze J, Schmuki P. Photoresponse in the visible range from Cr doped TiO_2 nanotubes. Chem Phys Lett. 2007;433:323–6.
10. Crawford GA, Chawla N. Porous hierarchical TiO_2 nanostructures: processing and microstructure relationships. Acta Mater. 2009;57:854–67.

11. Kim HJ, Lee KH. Dependence of the morphology of nanostructured titanium oxide on fluoride ion content. Electrochem Solid State Lett. 2009;12:C10–2.
12. Kunze J, Muller L, Macak JM, Greil P, Schmuki P, Muler FA. Time-dependent growth of biomimetic apatite on anodic TiO_2 nanotubes. Electrochim Acta. 2008;53:6995–7003.
13. Kodama A, Bauer S, Komatsu A, Asoh H, Ono S, Schmuki P. Bioactivation of titanium surfaces using coatings of TiO_2 nanotubes rapidly pre-loaded with synthetic hydroxyapatite. Acta Biomater. 2009;5:2322–30.
14. Liang YQ, Yang XJ, Cui ZD, Zhu SL. Effect of TiO_2 nanotube morphology on the formation of apatite layer in simulated body fluid. Curr Nanosci. 2010;6:256–61.
15. Buser D, Schenk RK, Steinemann S, Fiorellini JP, Fox CH, Stich H. Influence of surface characteristics on bone integration of titanium implants—a histomorphometric study in miniature pigs. J Biomed Mater Res. 1991;25:889–902.
16. Ellingsen JE. A study on the mechanism of protein adsorption to TiO_2. Biomaterials. 1991;12:593–6.
17. Popat KC, Leoni L, Grimes CA, Desai TA. Influence of engineered titania nanotubular surfaces on bone cells. Biomaterials. 2007;28:3188–97.
18. Peng L, Eltgroth ML, LaTempa TJ, Grimes CA, Desai TA. The effect of TiO_2 nanotubes on endothelial function and smooth muscle proliferation. Biomaterials. 2009;30:1268–72.
19. Brammer KS, Oh SH, Gallagher JO, Jin SH. Enhanced cellular mobility guided by TiO_2 nanotube surfaces. Nano Lett. 2008;8:786–93.
20. de Assis SL, Wolynec S, Costa I. Corrosion characterization of titanium alloys by electrochemical techniques. Electrochim Acta. 2006;51:1815–9.
21. Taddei P, Tinti A, Reggiani M, Monti P, Fagnano C. In vivo bioactivity of titanium and fluorinated apatite coatings for orthopaedic implants: a vibrational study. J Mol Struct. 2003; 651–653:427–31.
22. Popat KC, Eltgroth M, LaTempa TJ, Grimes CA, Desai TA. Decreased *Staphylococcus epidermis* adhesion and increased osteoblast functionality on antibiotic-loaded titania nanotubes. Biomaterials. 2007;28:4880–8.
23. Peng LL, Mendelsohn AD, LaTempa TJ, Yoriya S, Grimes CA, Desai TA. Long-term small molecule and protein elution from TiO_2 nanotubes. Nano Lett. 2009;9:1932–6.
24. Chow KT, Chan LW, Heng PWS. Formulation of hydrophilic non-aqueous gel: drug stability in different solvents and rheological behavior of gel matrices. Pharm Res. 2008;25:207–17.
25. Liang YQ, Yang XJ, Cui ZD, Zhu SL. Self-organized nanotubular layer on Ti–4Zr–22Nb–2Sn alloys formed in organic electrolytes. J Mater Res. 2009;24:3647–52.
26. Bauer S, Kleber S, Schmuki P. TiO_2 nanotubes: tailoring the geometry in H_3PO_4/HF electrolytes. Electrochem Commun. 2006;8:1321–5.
27. Yasuda K, Schmuki P. Formation of self-organized zirconium titanate nanotube layers by alloy anodization. Adv Mater. 2007;19:1757–60.
28. Feng XJ, Macak JM, Albu SP, Schmuki P. Electrochemical formation of self-organized anodic nanotube coating on Ti–28Zr–8Nb biomedical alloy surface. Acta Biomater. 2008;4:318–23.
29. Tsuchiya H, Macak JM, Ghicov A, Tang YC, Fujimoto S, Niinomi M, Noda T, Schmuki P. Nanotube oxide coating on Ti–29Nb–13Ta–4.6Zr alloy prepared by self-organizing anodization. Electrochim Acta. 2006;52:94–101.
30. Berger S, Tsuchiya H, Schmuki P. Transition from nanopores to nanotubes: self-ordered anodic oxide structures on titanium-aluminides. Chem Mater. 2008;20:3245–7.
31. Yasuda K, Schmuki P. Control of morphology and composition of self-organized zirconium titanate nanotubes formed in $(NH_4)_{(2)}SO_4/NH_4F$ electrolytes. Electrochim Acta. 2007;52: 4053–61.
32. Shankar K, Mor GK, Prakasam HE, Yoriya S, Paulose M, Varghese OK, Grimes CA. Highly-ordered TiO_2 nanotube arrays up to 220 μm in length: use in water photoelectrolysis and dye-sensitized solar cells. Nanotechnology. 2007;18:065707 (1–11).
33. Macak JM, Tsuchiya H, Schmuki P. High-aspect-ratio TiO_2 nanotubes by anodization of titanium. Angew Chem Int Ed. 2005;44:2100–2.
34. Lu MD, Yang SM. Synthesis of poly(3-hexylthiophene) grafted TiO_2 nanotube composite. J Colloid Interface Sci. 2009;333: 128–34.
35. Li ZJ, Hou B, Xu Y, Wu D, Sun YH. Hydrothermal synthesis, characterization, and photocatalytic performance of silica-modified titanium dioxide nanoparticles. J Colloid Interface Sci. 2005;288:149–54.
36. Antonel PS, Andrade EM, Molina FV. Copolymerization of aniline and *m*-chloroaniline. Chlorine addition and structure of the resulting material. React Funct Polym. 2009;69:197–205.
37. Choi HM, Bide M, Phaneuf M, Quist W, LoGerfo F. Dyeing of wool with antibiotics to develop novel infection resistance materials for extracorporeal end use. J Appl Polym Sci. 2004;92: 3343–54.
38. Saleema N, Farzaneh M, Paynter RW. Fabrication of TiO_2 mudonuts by sol-gel spin coating using a polymer mask. Appl Surf Sci. 2009;255:5837–42.
39. Janarthanan P, Yunus W, Bin Ahmad M. Thermal behavior and surface morphology studies on polystyrene grafted sago starch. J Appl Polym Sci. 2003;90:2053–8.
40. Chong ASM, Zhao XS. Functionalization of SBA-15 with APTES and characterization of functionalized materials. J Phys Chem B. 2003;107:12650–7.
41. Kristensen EME, Nederberg F, Rensmo H, Bowden T, Hilborn J, Siegbahn H. Photoelectron spectroscopy studies of the functionalization of a silicon surface with a phosphorylcholine-terminated polymer grafted onto (3-aminopropyl)trimethoxysilane. Langmuir. 2006;22:9651–7.
42. Martin HJ, Schulz KH, Bumgardner JD, Walters KB. XPS study on the use of 3-aminopropyltriethoxysilane to bond chitosan to a titanium surface. Langmuir. 2007;23:6645–51.
43. Lopez N, Gomez-Segura J, Marin RP, Perez-Ramirez J. Mechanism of HCl oxidation (Deacon process) over RuO_2. J Catal. 2008;255:29–39.
44. Xu QG, Yuan XB, Chang J. Self-aggregates of cholic acid hydrazide-dextran conjugates as drug carriers. J Appl Polym Sci. 2005;95:487–93.
45. Yu CY, Cao H, Zhang XC, Zhou FZ, Cheng SX, Zhang XZ, Zhuo RX. Hybrid nanospheres and vesicles based on pectin as drug carriers. Langmuir. 2009;25:11720–6.
46. Ajima K, Yudasaka M, Murakami T, Maigne A, Shiba K, Ijima S. Carbon nanohorns as anticancer drug carriers. Mol Pharm. 2005;2:475–80.